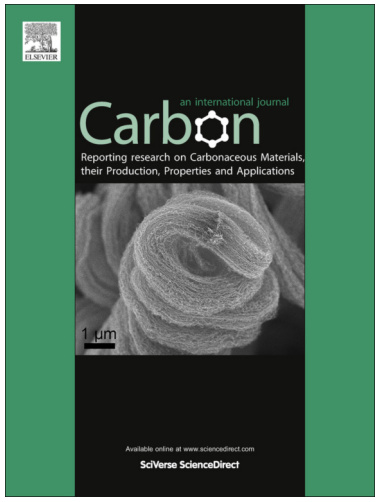

Towards the understanding of the graphene oxide structure: How to control the formation of humic- and fulvic-like oxidized debris

Iluminada Rodriguez-Pastor, Gloria Ramos-Fernandez, Helena Varela-Rizo, Mauricio Terrones, Ignacio Martin-Gullon

PII: S0008-6223(14)01177-4
DOI: http://dx.doi.org/10.1016/j.carbon.2014.12.027
Reference: CARBON 9560

To appear in: *Carbon*

Received Date: 21 July 2014
Accepted Date: 4 December 2014

Please cite this article as: Rodriguez-Pastor, I., Ramos-Fernandez, G., Varela-Rizo, H., Terrones, M., Martin-Gullon, I., Towards the understanding of the graphene oxide structure: How to control the formation of humic- and fulvic-like oxidized debris, *Carbon* (2014), doi: http://dx.doi.org/10.1016/j.carbon.2014.12.027

Towards the understanding of the graphene oxide structure: How to control the formation of humic- and fulvic-like oxidized debris

Iluminada Rodriguez-Pastor[1], Gloria Ramos-Fernandez[1], Helena Varela-Rizo[1], Mauricio Terrones[2], Ignacio Martin-Gullon[1*]

[1]Chemical Engineering Department, University of Alicante, Alicante 03690, Spain

[2]Department of Physics, Department of Chemistry, Department of Materials Science and Engineering & Center for 2-Dimensional and Layered Materials, The Pennsylvania State University, University Park, PA 16802-6300; and Institute of Carbon Science and Technology, Shinshu University, Wakasato 4-17-1, Nagano 380-8553, Japan

Abstract

Former structural models of graphene oxide (GO) indicated that it consists of graphene-like sheets with oxygen groups, and no attention was paid to the resulting sheet size. We now provide evidence of the complex GO structure consisting of large and small GO sheets (or oxidized debris). Different oxidation reactions were studied. $KMnO_4$ derived GO consists of large sheets (20-30 wt. %), and oxidized debris deposits, which are formed by humic- and fulvic-like fragments. Large GO sheets contain oxygen groups, especially at the edges, such as carbonyl, lactone and carboxylic groups. Humic-like debris consists of an amorphous gel containing more oxygenated groups and trapped water molecules. The main desorbable fraction upon heating is the fulvic-like material, which contains oxygen groups and fragments with high edge/surface ratio. $KClO_3$ in HNO_3 or the Brodie method produces a highly oxidized material but at the flake level surface only; little oxidized debris and water contents are found. It is noteworthy that an efficient basal cutting of the graphitic planes in addition to an effective intercalation is caused by $KMnO_4$, and the aid of $NaNO_3$ makes this process even more effective, thus yielding large monolayers of GO and a large amount of humic- and fulvic-like substances.

* Corresponding author. Tel: +34 96 5903867. E-mail: gullon@ua.es

1. Introduction

Graphene (an individual sheet of sp^2 hybridized carbon) can be produced by bottom-up approaches, that include epitaxial growth techniques, polymerization of molecules [1-3], or top-down methods consisting of delaminating graphite crystals [4]. However, the latter method could result in different graphene-like materials including pristine graphene (PG), produced through liquid phase exfoliation [5, 6], and graphene oxide (GO), synthesized by chemical intercalation and the subsequent oxidation of graphitic materials (e.g. graphite [7], carbon nanotubes [8], carbon nanofibers [9]).

GO also appears to be an excellent precursor for synthesizing more complex and hybrid graphene-based materials[10] at affordable costs. The GO structure consists of a graphene layer modified with oxygen functional groups decorating the basal plane and edges [11]. It is noteworthy that some of the unique graphene properties are lost due to the presence of these functional groups and defects produced during the oxidation, such as its electronic structure, converting GO into an insulator. However, some of these properties could be partially recovered by a reduction treatment, and the resulting material is called reduced graphene oxide, rG-O [12]. In the past few years, there was an agreement that GO was scalable in the ton-scale [13], and consequently, emerged as a precursor for an affordable form of graphene suitable for high-volume applications, such as composites [14] and energy storage components [15]. More recently, the interest in GO synthesis remains and companies working in biotechnology and electrochemistry are now showing interest [11]. In addition, high-shear liquid exfoliated PG offers an alternative to the bulk synthesis of graphene-like materials [6] which could also be used in the fabrication of composites [16] and batteries [17]. An advantage of GO when compared to pristine graphene flakes lies in the presence of functional groups that make it ideal for applications involving composites in which matrix-filler bonding is preferred [14, 18].

Therefore, the control in the fabrication of novel hybrid materials and 3-dimensional structures[10] require the development of an adequate and reliable synthesis model which could deep our knowledge in understanding the detailed structure of GO and its reduced forms. Over the past decades, different models for the structure of graphite

oxide were proposed, mainly consisting of a homogeneous oxidized structure [19-22]. The model proposed by Lerf-Klinowski appears to be the most accepted accounting for the structure of graphite oxide [23, 24], and was subsequently adopted to explain the structure of GO, based on a non-stoichiometric system containing intercalated water and two kinds of regions: *aromatic non-oxidized domains*, and *areas containing oxygen groups*, such as epoxy and tertiary alcohols on the basal plane, responsible of producing a flat layer structure, and carboxylic groups located at the edges of these sheets. Subsequent studies indicated the presence of carboxyl and carbonyl groups at the edges [25]. Unfortunately, this general structural model for GO does not take into account the influence of the graphitic parent material or the influence of the oxidation method [25]. In this context, some authors pointed to different behaviors of GO depending on the production method. Seredych *et al.* [26] compared GO obtained by Hummers-Offeman [7] and by Brodie [27] methods and found clear differences in chemical surface which resulted in different adsorption capacities of ammonia. Chua *et al.* [28] also observed differences in the structural and electrochemical properties of GO depending on the use of permanganate or chlorate using the Staudenmaier [29], Hofmann[19] , Hummers [7] and Tour[30] oxidations. Therefore, the graphitic source as well as the oxidation method should be carefully considered in order to establish a precise control of the GO structure.

Recently, a novel approach for synthesizing GO has emerged. Rourke *et al.* [31] reported that GO directly obtained after the oxidation of a graphitic material exhibits a more complex structure consisting of two main entities: functionalized graphene-like sheets and oxidized debris (OD) strongly adhered to these flat entities. This assumption is based on results obtained using carbon nanotubes [32, 33] or carbon fibers [34] as parent graphitic materials. OD consist of large poly-aromatic molecules with high amount of oxygen groups anchored to the edges, that also act as a surfactant able to disperse clean GO sheets. Therefore, it appears that clean GO sheets are not heavily oxidized (C/O ratio is much higher when compared to OD), and as a consequence, clean G-O sheets are not fully soluble in water, and are more electrically conducting. Clean GO sheets represented around 2/3 of the parent GO, while OD are the rest 1/3. More recently, it was reported that the amount of OD formed is similar, around 1/3 of initial GO, regardless of the oxidation production method [35]. As the presence of debris

affect GO properties [31, 35-38] , it is important to determine the OD structure and be able to assess a correct interpretation of the GO structure.

Published work using multi-walled carbon nanotubes (MWCNTs) as the graphitic precursor material identified debris with fulvic-like structures [39]. More recently, the degradation of GO in water has been reported to be associated with the formation of humic-like entities [40]. In soil science, humic and fulvic acids, together with humin, are formed by the degradation of biomolecules. Humic and fulvic acids differ in molecular weight (higher for humic acids), number of functional groups (carboxyl, phenolic OH) and solubility. Humic acids are not soluble in water under acidic conditions (pH<2) while fulvic acids are soluble in water under all pH conditions; humin is insoluble at any pH. Based on this property, humic and fulvic acids are generally separated by base and acid washing procedures. A similar approach is employed to remove debris from the GO surface [31, 36].

In this work, we synthetized graphene oxide from natural expanded graphite through four different methods, and the samples were characterized in terms of as produced GO, washed-GO (clean sheets) and the humic fraction of OD (denoted as OD-humic). In particular, transmission electron microscopy (TEM), X-ray photoelectron spectroscopy (XPS), X-ray diffraction (XRD), thermogravimetry coupled to mass spectrometry (TG-MS) and Raman spectroscopy were used to characterize the samples. Four different reaction methods, involving the use of different intercalation and oxidation agents were used: Hummers-Offeman (denoted as HO, and involving the treatment with $KMnO_4/NaNO_3/H_2SO_4$) [7], modified Hummers-Offeman (denoted as HOm, including $KMnO_4/H_2SO_4$) [8, 9], Brodie (denoted as Br, considering $KClO_3/HNO_3$) [27, 41] and Staudenmaier (denoted as St, and involving $KClO_3/H_2SO_4/HNO_3$) [29]. These results are used to propose a new model for GO.

2. Experimental

2.1.Materials

Natural expanded graphite BNB90 was kindly supplied by Timcal (Bodio, Suiza). This material exhibits an average flake thickness of 35 nm and dimensions of 50 μm.

$KMnO_4$, $KClO_3$ and $NaNO_3$ were purchased from Sigma Aldrich. H_2SO_4 (95%), H_2O_2 (33 vol %) and fuming HNO_3 were supplied by VWR International.

2.2. Production methods of GO

Hummers-Offeman

1 g of graphite, 200 ml of H_2SO_4 and 0.5g of $NaNO_3$ were mixed and stirred at room temperature. After 3 h, 3g of $KMnO_4$ were added and the suspension was stirred for 2 h. Subsequently, the temperature was increased to 60ºC and kept for 1 h. Once the reaction was completed, it was cooled down to room temperature, and poured into 400 ml of cold water with 40 ml of H_2O_2, in order to prevent MnO_2 precipitation. After several water washing/filtration procedures, the solid GO product was dried overnight at 65ºC. This sample was named GO-HO.

Modified Hummers-Offeman

1g of graphite and 200 ml of H_2SO_4 were mixed and stirred at room temperature. After 3 h, 5g of $KMnO_4$ were added to the suspension and stirred for 2 h. From this step, the same procedure of Hummers-Offeman method was applied. The corresponding product is labeled as GO-HOm.

Brodie

1g of graphite was suspended in 80 ml of HNO_3 and stirred. At this point, 8.5 g of $KClO_3$ were added in aliquots over a period of 6 h, and the stirring continued for 18 h. Then, the solution was heated to 60ºC for 6 h and, finally, cooled down to room temperature. The mixture was poured in 400 ml of cold water. After subsequent water washing/filtration steps, the product was dried overnight at 65ºC. This sample is labeled as GO-Br.

Staudenmaier

1g of graphite was added to a suspension of 30 ml of HNO_3 and 60 ml of H_2SO_4. The mixture was stirred and 8.5 g of $KClO_3$ were added in aliquots over a period of 6 h, and the stirring continued for 18 h. The method then followed the same procedure as the Brodie method. This sample was labeled as GO-St.

GO samples (1 g each) were thermally reduced through microwave furnace treatment 800 W for 120 s, getting the corresponding reduced graphene oxide (rGO).

2.3.Separation of OD

A suspension of G-O in water (1 mg/ml) was prepared by exfoliating through bath sonication for 1 h. A solution of NaOH 6N was then added while stirring until reaching a pH of 12, and then the mixture was refluxed for an hour. After cooling to room temperature the mixture was centrifuged at 9000 rpm for 10 min, and separated in 2 fractions, a supernatant (SP1) and a black solid (solid 1). The SP1, containing the OD was reprotonated up to pH 2 by adding HCl 1N, which resulted in a colorless solution and a precipitated solid. These two fractions were separated by centrifugation at 9000 rpm for 10 min. The colorless solution contains the fulvic-like molecules suspended in water, and the solid corresponds to humic-like fragments.

Solid 1, obtained from the first NaOH washing, was exfoliated using an ultrasonication tip (30 W for 2 hours, in 60 s ON- 30 s OFF intervals), neutralized with HCl (1M) and refluxed for 1h. Once again, a supernatant (SP2) and a solid (solid 2) were separated by centrifugation at 9000 rpm for 1h. Solid 2 was washed with water and centrifuged at 9000 rpm for 10 min, resulting in a supernatant (SP3) and a black solid (solid 3). Solid 3 consisted of the cleaned GO free of debris. SP2 and SP3 were mixed and brought to pH 2 with HCl (1M). Subsequent centrifugation at 9000 rpm for 10 min separates a colorless solution and a black solid, equivalent to residual fulvic-like and humic-like products, respectively. GO free of debris is labeled as washed-GO and humic–like structures as OD-humic.

2.4.Characterization

GO crystals from a 0.1 mg/mL suspension in isopropanol morphology was explored by high-resolution transmission electron microscopy (HRTEM, JEOL JEM-2010) and the number of layers was identified by both platelet edge observation and electron diffraction patterns. Non-exfoliated GO powder was used for the rest of the characterization. Raman spectra were recorded on a LabRam (Jobin-Ivon) using a 532 nm excitation and a minimum of 5 spectra were taken for each sample, in order to get average Raman shifts and intensity values. X-ray photoelectron spectroscopy (XPS) was carried out with a K-Alpha Spectrometer (Thermo-Scientific), and in order to calculate the superficial atomic ratio of C and O, and quantify the functional groups, the integration of the survey spectra was performed. Thermogravimetric and mass

spectrometry analysis (TG-MS) was also performed using a Mettler Toledo TGA/SDTA851e/LF/1600 coupled with a Thermostar GSD301T in order to measure the weight loss and gas evolution from the thermal decomposition of samples of GO, washed-GO and OD-humic like substances from different production methods. The experiments were carried out under He atmosphere, from room temperature to 1000 ºC with a heating rate of 20 ºC/min, and m/z = 18 (H_2O), 28 (CO) and 44 (CO_2) were integrated and quantified by means of $CaC_2O_4 \cdot H_2O$ standard. XRD was carried out using a Bruker D8-Advance equipment, with Göebel mirror, and the acquisition was done with a step of 0.05º. TG-MS runs were duplicated per sample, and the results were always consistent; below 2.5% for m/z 18, 28 and 44.

3. Results and discussion

3.1.Influence of the production method

TEM images of the parent natural expanded graphite (Figure S1) show a high degree of crystallinity as well as faceted high-sized graphite flakes, usually containing a number of layers above 10-20 layers according to the edge width and transparency. This fact is consistent with the crystallographic parameters obtained from XRD from the parent graphite (Figure S2), which gives an Lc value above 60 nm. The intercalation and oxidation treatment clearly reduces the number of layers (Figure 1). GO-HO and GO-HOm layers have similar dimensions, finding uniform sheets (average size *ca.* 1-3 μm). A high yield of monolayers is achieved when using $NaNO_3$ (GO-HO sample), over 50% of the analyzed sheets exhibited characteristic single layer electron diffraction pattern (ESD). As an example, Figure 1.a corresponds to a single layer sheet of GO-HO. However, for GO-HOm, only few single layer sheets (below 15% of the observed sheets) where found on the exploration, and Figure 1.b shows a representative example of these sheets. With respect to GO-Br and GO-St, we could not find any mono- or bi-layer sheets, and quite often non exfoliated large graphite oxide flakes were found (non-transparent); partially exfoliated GO consisted of multilayer nanoplatelets with lateral dimensions below 1 μm..

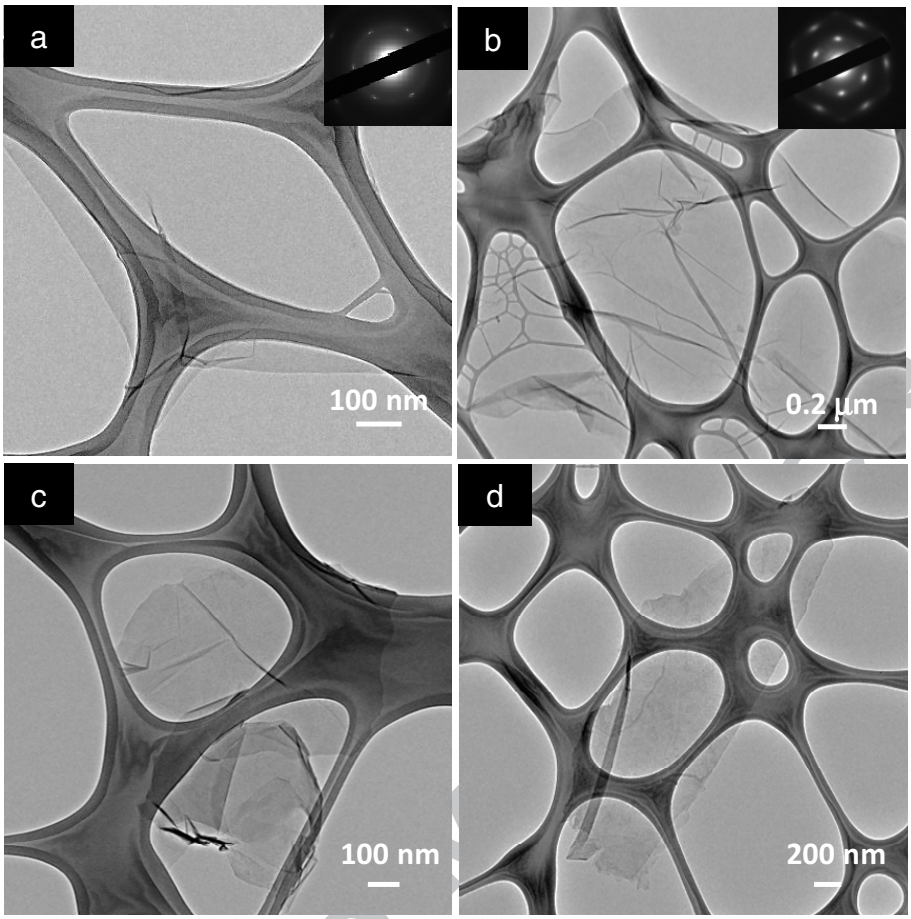

Figure 1. TEM images of GO sheets produced by different methods: (a) GO- HO, (b) GO-HOm, (c) GO-Br and (d) GO-St

Raman spectra of parent graphite and GO are shown in Figure 2. In particular, the spectrum of graphite exhibits a sharp and intense G-band (1580 cm^{-1}), a low intensity D-band (1350 cm^{-1}) and D'-band (1620 cm^{-1}), which indicates the high degree of crystallinity of graphite used. The intercalation and oxidation of graphite causes similar changes according to Raman spectroscopy. The intensity of G-band decreases, form a broad peak together with the D' peak (denoted G-D' band) for all GO samples, with different asymmetries depending on the relative contribution of G and D' peaks. On the other hand, the D-band becomes also broader and more intense, as a result of the introduction of oxygen groups and other structural defects in the graphitic structure. This effect is more noticeable in GO-HO and GO-HOm samples, and it indicates that the degree of crystallinity has decreased considerably. In addition, the D'- and G-bands overlap, thus yielding to a broader and asymmetric peak, as observed in graphite intercalation compounds [42]. The largest Raman shifts displacement for the G-D' overlapped bands corresponds to the Brodie sample, which means that the oxidation

reaction mechanism and the number of defects introduced in the material are different to those introduced by $KMnO_4/H_2SO_4$ graphite treated samples. Representative Raman shifts for the different samples, as well as the intensity D/G ratio, are shown in Table 1. Regarding the 2D-band (2700 cm^{-1}), it is well-defined in the parent graphite sample, due to the high degree of crystallinity of the material. Further oxidation broadens this peak and reduces its intensity, especially for the $KMnO_4$ treated samples. This transformation is characteristic of the GO spectrum [43] and suggests a significant reduction of the size of sp^2 domains [44]. The 2D peak shape does not change significantly for GO-Br and GO-St, as well as D+G peak 2950 cm^{-1}), thus implying that the aromatic structure of the oxidized material is somewhat preserved with these methods and less defects or functional groups were introduced. It must be reminded that the Raman signal collects information from a circular spot of *ca.* 1 μm, from the surface and a few layers underneath (skin depth) [45].

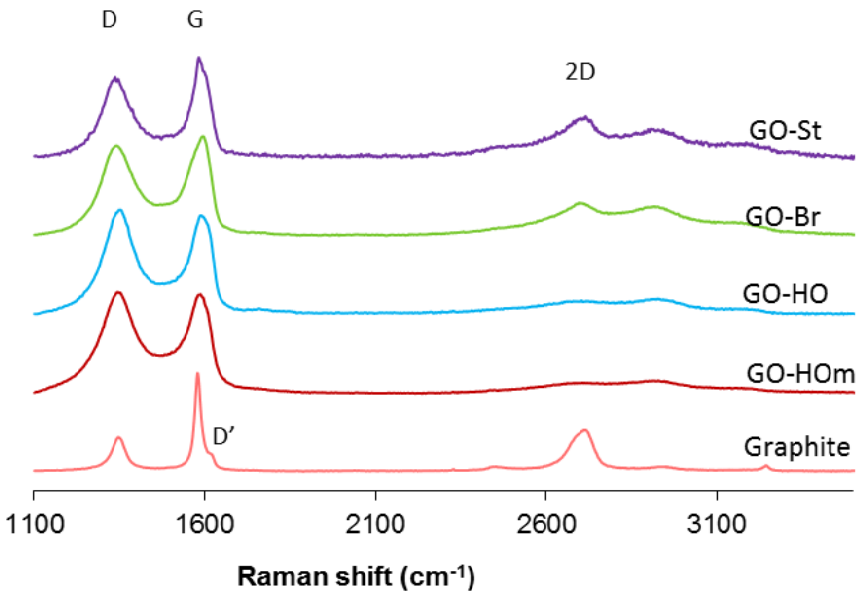

Figure 2.Raman spectra of graphite, GO-HO, GO-HOm, GO-Br and GO-St

Table 1. D, G-D' and 2D peak Raman shifts, and D/G-D' intensity ratio, for graphene oxide samples from different oxidation methods. Shown values are extracted from average values of 5 representative spectra.

	Raman Shifts (cm^{-1})			I_D/I_G
	D peak	**G-D' peak**	**2D peak**	
Graphite	1349	1580	2711	0.35
GO-HOm	1345	1588	2706	1.02
GO-HO	1350	1589	2704	1.06
GO-Br	1341	1597	2697	0.91
GO-St	1337	1582	2715	0.80

TG-MS results are shown in Figure 3 and Table 2, and reflect the differences of the G-O synthesis method. For example, GO-HO and GO-HOm reveal thermograms with three characteristic weight loss steps, usually found in GO obtained by this method [8, 46]. The initial step ranges from room temperature to 140ºC and corresponds to physisorbed H_2O (m/z=18). A second weight loss is observed at 200ºC, where the quantified signals of m/z=18, 28 (CO) and 44 (CO_2) are detected. For GO-HO, the qualitative signals of m/z=30 and 46 (NO and NO_2) are also detected due to the oxidation of nitrogen groups. From 200ºC to 280ºC, m/z=64 (SO_2) is clearly shown and it is due to the decomposition of organosulfates [47], with minor contributions of H_2O. The weight loss above 400ºC is caused by the slow and steady decomposition of the sp^2 hybridized carbon skeleton [48].

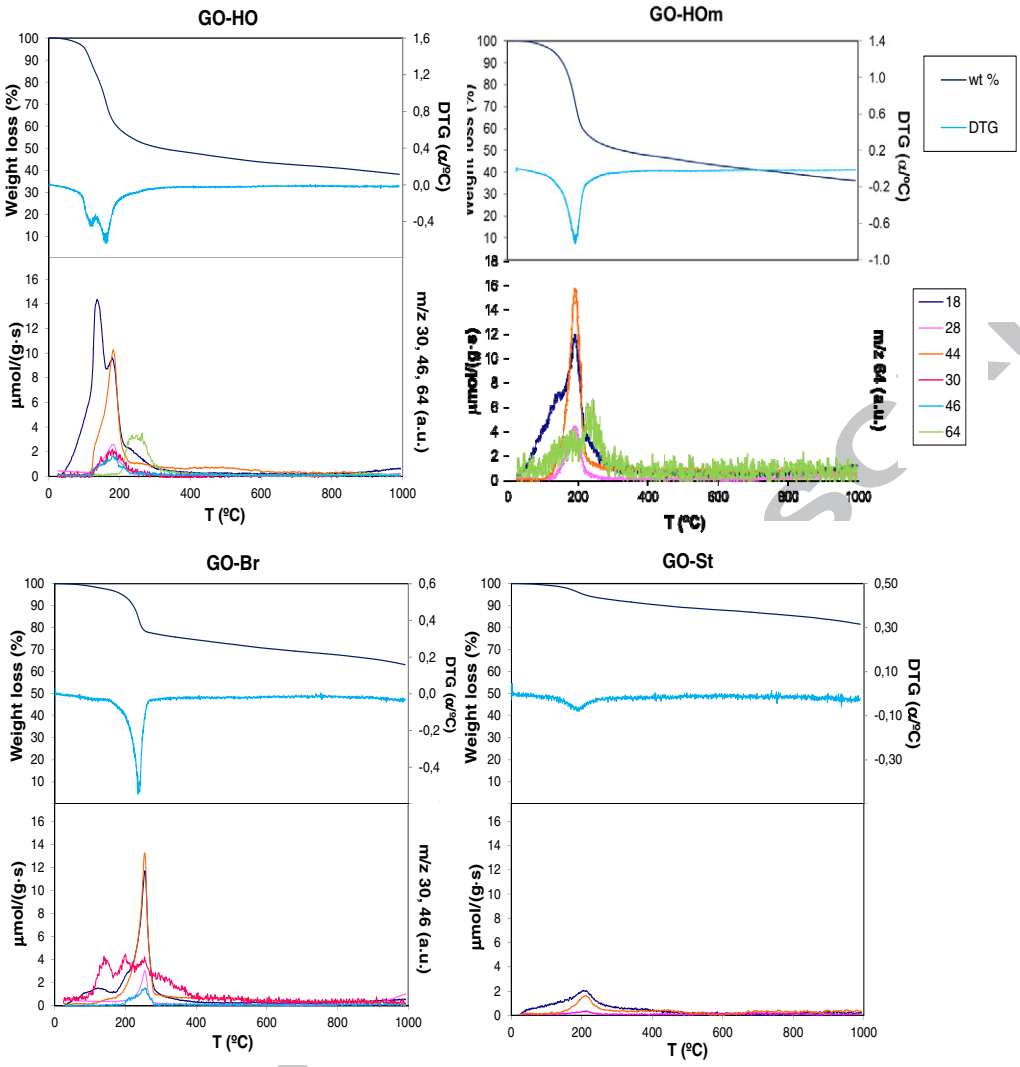

Figure 3. TG-MS of GO-HO, GO-HOm, GO-Br and GO-St

GO-St shows a similar thermogram when compared to the Hummers-Offeman method (similar temperature peak in DTG), with lower weight loss. Moreover, m/z=30, 46 and 64 are not detected possibly due to the small weight loss values. Finally, the thermogram of GO-Br shows the most significant differences. The first weight loss, due to water evaporation within the 100-180ºC range is much lower and negligible with respect to the $KMnO_4$ treated G-O samples, thus confirming that water is not present (trapped) for GO-Br. The most prominent loss in the TG plot is delayed with respect to other methods, at temperatures >200ºC, the release of CO_2 and H_2O and small contributions of CO occur, and at m/z = 46 some nitrogen groups are liberated due to

the presence of HNO_3. From 100 to 380ºC, m/z=30 was also observed. The overall weight loss from room temperature to 500ºC is 55% for GO-HO and GO-HOm, 28% for GO-Br and 11% for GO-St. Therefore, the Brodie and, especially the Staudenmaier methods are less effective for introducing functional groups when compared to the Hummers-Offeman methods (e.g. less degree of the intercalation/oxidation reaction, as confirmed by TEM and Raman). Additionally, it is also noticeable the negligible physisorbed water content for GO-Br, which is expected to be located in between the oxidized layers. The quantification of H_2O, CO and CO_2 in wt. % with respect to the initial GO at the beginning of the TGA runs, is shown in Table 2, and clearly states a high CO_2 content for GO-HO, GO-HOm and GO-Br. H_2O content is high for GO-HO and GO-HOm, and lower but not insignificant for GO-Br. Lower water content in GO-Br and GO-St can be due to the absence of organosulfate groups. On the other hand, the sum of gravimetric amounts of H_2O, CO and CO_2 nearly matches with the total weight loss for GO-Br and GO-St, thus indicating that all the decomposition gas products are determined. However, around 20% weight loss of chemical compounds could not be accurately determined in GO-HO and GO-HOm. This could be due to the presence of non-oxygenated molecules such as SO_2 and others liberated from the G-O structure.

Table 2. Quantification of the evolved decomposition products of GO-HO, GO-HOm, GO-Br and GO-St

Sample	**H_2O (%)**	**CO (%)**	**CO_2 (%)**
GO-HOm	13.6	3.8	18.5
GO-HO	13.8	2.9	21.2
GO-Br	7.8	2.3	20.0
GO-St	4.1	0.9	5.8

XPS spectra (Figure 4) were fitted to Gaussian functions and FWHM of peaks were fixed at a maximum limit of 2eV. The C1s binding energies at 284.5 and 289 eV correspond to C=C aromatic and carboxylic groups, respectively; note there is not clear agreement in the literature about how to assign bands between 285 and 287.6 eV [44, 49, 50]. The present work follows the same criteria used by Ganguly et al [44]. The band at 285.5 eV indicates either hydroxyl groups or sigma C-C sp^3. The band at *ca.* 286.5 eV is indicative of ether, epoxy (sp^3 C-O-C sp^3), while the binding energy at 287.5 eV reveals carbonyl, lactone and similar groups. The signal located at 290.5 eV

may appear, and it is assigned to (π→π*) shakeup satellite, corresponding to delocalized πconjugation. For comparison, the parent natural graphite shows a prominent C=C peak as well as the (π→π*) shakeup satellite, both characteristics of aromatic carbon structures. This material also contains small contributions from both C=O and C-OH/C-Csp^3. These groups could derive from the chemical intercalation of natural graphite in the expanded graphite production process. The ratio of oxygen groups with respect to the aromatic C=C increases for all GO samples using different synthesis methods. After fitting the spectra, the C/O ratio denotes a higher oxidation of GO-HOm when compared to GO-HO, and this can be explained by the lower ratio $KMnO_4$:graphite used in GO-HO. The peak deconvolution indicates a very high contribution of carbonyl-lactone groups as well as ether-epoxy species, and a low contribution of carboxylic groups. The low C/O ratio of these two methods is caused by the combination of two effects, oxygen groups introduced to GO and the amount of water incorporated to GO, as shown by TG-MS.

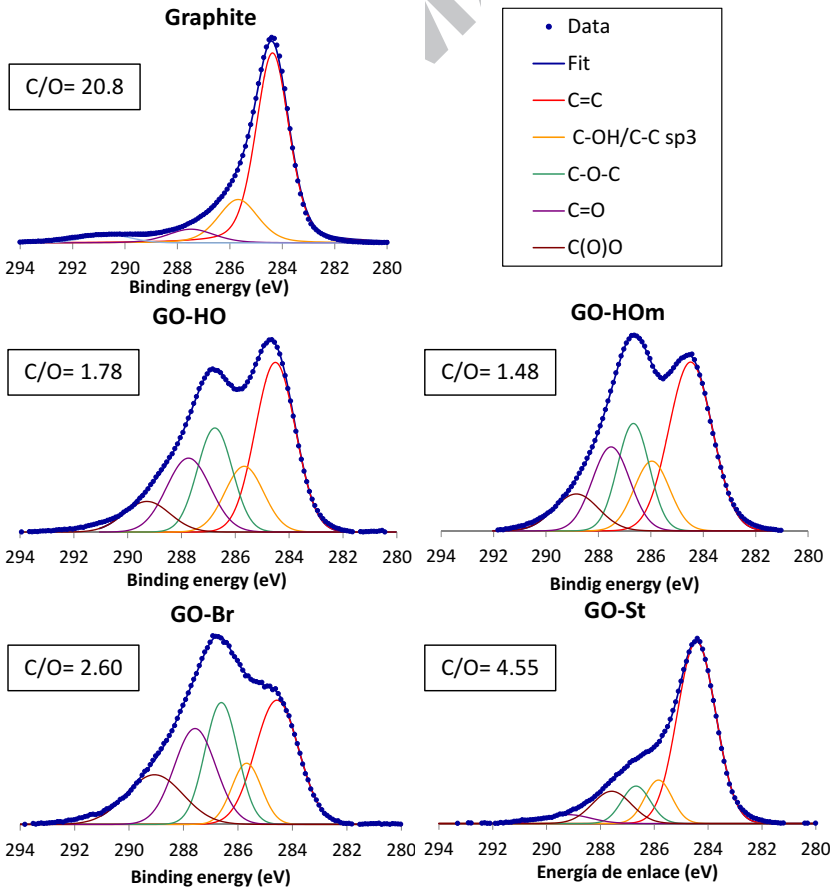

Figure 4. XPS C1s spectra of graphite, GO-HO, GO-HOm, GO-Br and GO-St

According to the C1s XPS spectra, the GO-Br seems to be the most oxidized sample, which contrasts previous results shown by TEM, Raman spectroscopy and TG-MS. This particular sample exhibits lower proportion of C=C bonds and a larger amount of carboxylic groups, when compared to both Hummers-Offeman derived GO samples. In addition, the GO-Br sample shows a high proportion of sp^3 C-O-C bonds. Moreover, the C/O ratio is larger for the Brodie sample (2.60). Therefore, GO-HOm and GO-HO have less superficial oxidized carbon atoms when compared to GO-Br, but more water intercalated than the Brodie sample (also observed by the TG-MS results shown in Figure 3 and by the C/O values). The experimental results seem to indicate than $KClO_3/HNO_3$ introduce functional groups only on the superficial outer layers of graphite, especially carboxylic and ether-epoxy, and it is not intercalating as there is no water trapped. The high carbonyl/lactone groups found in the Hummers-Offeman samples can be explained by the chemical scissors effect of $KMnO_4$, opening basal planes and leaving carbonyl groups behind[8]. Finally, GO-St is the less effective oxidation method. The results presented here are also consistent with other works [28, 51], thus concluding that the use of $KMnO_4$ is more suitable for the oxygen introduction when compared to $KClO_3$.

XRD results (Figure 5) confirm these last statements. Figure 5a shows the XRD plots of different GO samples, and Figure 5b shows those of the corresponding exfoliated thermally reduced graphene oxide (rGO), obtained after 2 minutes microwave reduction treatment. GO plots show that $KMnO_4$ samples exhibit a single displaced peak at around 10 degrees arising from large interlayer spacing, indicative of a satisfactory intercalation treatment. On the other hand, Staudenmaier sample shows the graphite (002) reflection at 26.5º, as if intercalation had not taken place, and the Brodie sample reveals two peaks that show partial intercalation of the graphite crystals; intercalation only occurred in some preferential layers. Interestingly, X-ray diffraction pattern corresponding to rGO-HO shows a full exfoliation (most of the material consist of exfoliated monolayers), thus confirming the satisfactory intercalation, whereas both the Brodie and the modified Hummers and Offeman exfoliated samples still show a small (002) graphite reflection at *ca.* 26º, indicating that the intercalation did not occur at every layer of the parent material. It seems that $NaNO_3$ is necessary for the successful intercalation/exfoliation of graphite; rGO-HO sample shows no (002) peak, whereas in

rGO-HOm the (002) peak reappeared. Finally, rGO-St also showed a sharp (002) graphite peak, as expected.

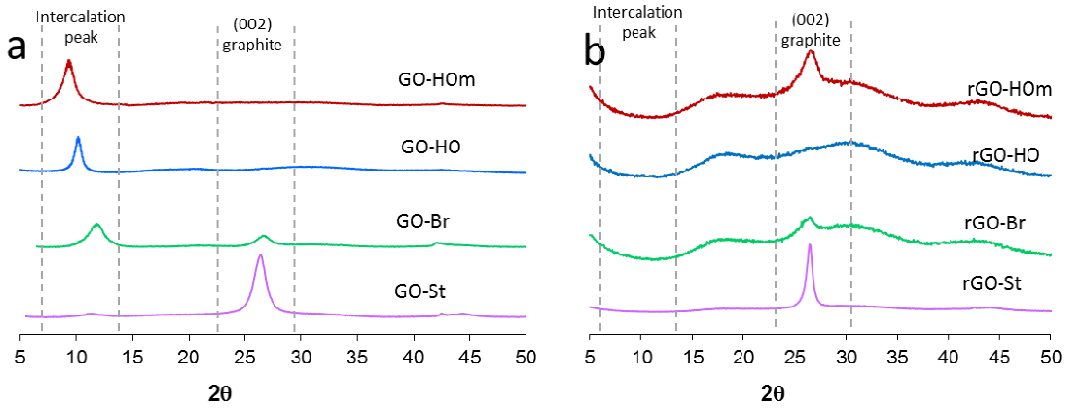

Figure 5. XRD plots of graphene oxide (a) and reduced graphene oxide samples by microwave treatment (b), for the different production methods.

3.2.Formation of oxidized debris

According to the protocol established in the experimental section, G-O clean sheets and OD were separated. Washed-GO and OD-humic gravimetric fractions were characterized for all samples; note that the OD fulvic fraction is undetermined. Additional characterization by TEM, TG-MS and XPS was performed to study the GO-HOm washed G-O sheets and OD-Humic.

Figure 6 shows the differences in the amount of washed-GO and OD-humic depending on the production method. The higher amount of OD-humic is formed by Hummers-Offeman and modified Hummers-Offeman methods, thus demonstrating that the couple $KMnO_4/H_2SO_4$ acts in a very different way as $KClO_3/HNO_3$, with nearly no OD formation for the latter. In addition, H_2SO_4 wets the surface and intercalates in between the graphite layers, thus making possible the access of $KMnO_4$ which cuts effectively the basal planes leaving carbonyl groups on the new formed edges [8]. This chemical scissors reaction (using $KMnO_4$) forms either large-single sheets, or small (humic) and very small (fulvic) entities, which are all fully oxidized at the edges. On the contrary, the Brodie GO samples are only oxidized superficially, with oxygenated groups on some of the basal planes (no scissors effect). It is significant the effect of $NaNO_3$ on the

graphitic layers, although it is still not well understood. As the cutting effect is due to $KMnO_4$ [8], the higher amount of OD-humic and lower for washed-GO with $NaNO_3$ indicates that nitrate clearly helps $KMnO_4$ intercalation between the layers, along with H_2SO_4, thus making $KMnO_4$ much more effective. The remaining material, not-quantified, is expected to be OD-fulvic, and water, which could be trapped within G-O.

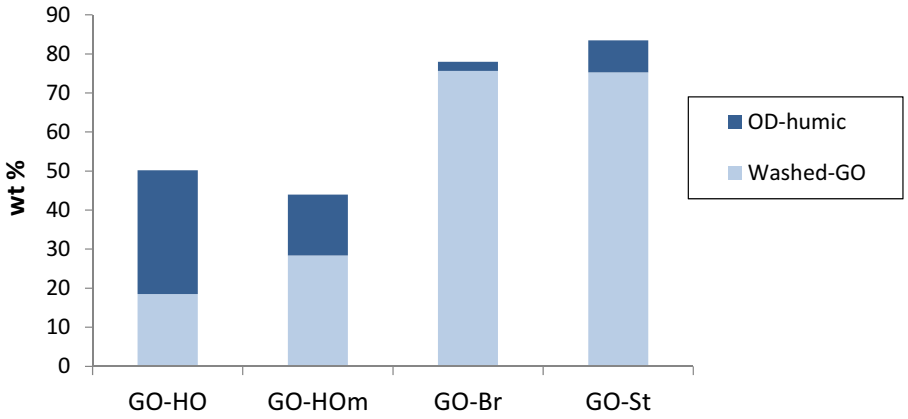

Figure 6. Mass balance of washed-GO and OD-humic obtained from GO-HOm, GO-HO, GO-Br and GO-St (wt. % respect to initial G-O)

It is noteworthy that the washed-GO fraction is the most abundant for the Brodie derived GO, nearly 80%, with a minimal OD-humic portion, less than 2%. It is surprising to observe this small OD formation when the superficial oxidation was the highest (see Figure 4). The $KClO_3/HNO_3$ is not effective when penetrating in between the layers, the oxidation is mainly occurring on top of the flake, and clearly $KClO_3$ does not have the cutting effect that $KMnO_4$ has.

GO-HOm derived washed-GO and OD-humic were selected for further characterization. The washed-GO and OD-humic materials of different nature were studied by TEM (see Figure 7 a-b and c-d, respectively). Washed-GO is a crystalline material and preserves the laminar graphene-like structure, in spite of being more aggregated and wrapped than the original GO. On the contrary, OD-humic does not exhibit any laminar structure and appears as an amorphous gel, as it corresponds to an aggregation of macromolecules.

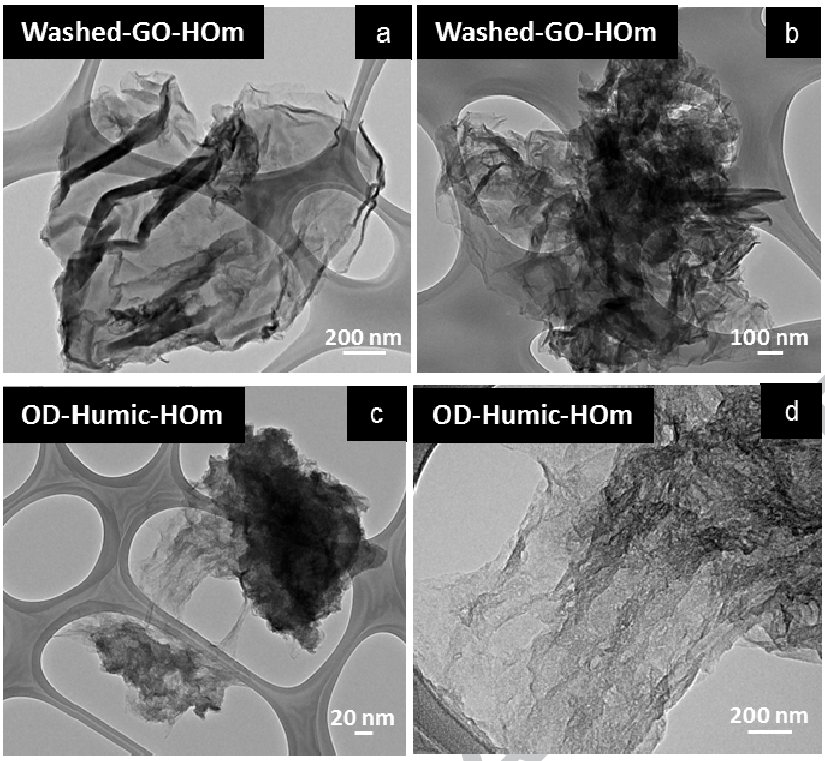

Figure 7. TEM images of (a) and (b) washed-GO, and (c) and (d) OD-humic at different magnifications

Differences in TG-MS are shown in Figure 8. Thermograms of washed-GO and OD-humic do not present the pronounced weight loss at 180 ºC. This fact suggests that the steep weight loss observed in GO-HOm around this temperature is due to OD fulvic fraction, plus physisorbed trapped water, in addition to oxygen groups and organosulfates. Similar results were reported by other authors [31]. Furthermore, weight loss plots show a smooth profile, with weight loss values appearing at 500ºC (20% for washed-GO and 30% for OD-humic, whereas 45% for GO-HOm). This difference corresponds to the sum of water and CO detected in Figure 3. Table 3 shows that the little amount of water and CO evolved while CO_2 values keep stable (see Table 2). With respect to washed-GO and OD-humic, both samples contain similar amounts of CO_2 and a similar profile evolution versus temperature, with a first maximum at 200 ºC. However, the water evolution amount is different, as well as its profile: washed-GO displays a dual peak at *ca.* 100 and at *ca.* 200ºC, while OD humic shows a single and broader peak at *ca.* 160ºC. Apparently, water is clearly associated to the polar structure of humic substances. It is also important to note the negligible evolution of CO from those fractions at medium range temperatures.

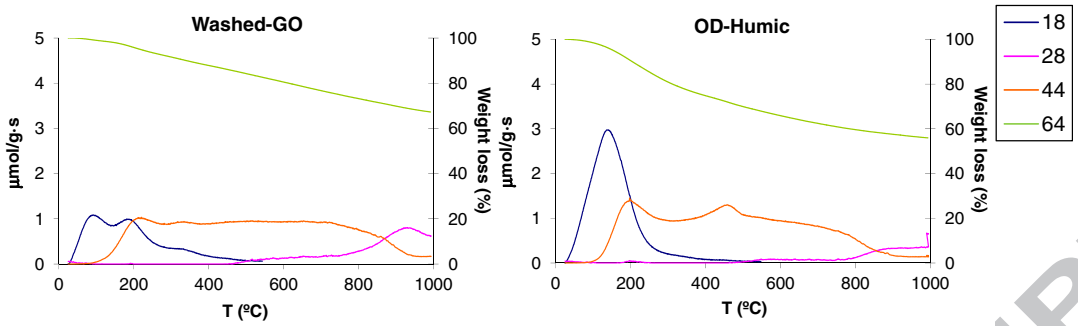

Figure 8. TG-MS of washed-GO and OD-humic

Table 3. TG-MS quantification of washed-GO and OD-humic

Sample	H_2O (%)	CO (%)	CO_2 (%)
Washed-GO	2.6	0.7	16.5
OD-humic	4.1	0.3	18.3

XPS spectra shown in Figure 9 reveal the great difference among the oxidation level of the parent GO-HOm, and the derived washed-GO and OD-humic. These curves confirm the lower oxygen content in GO after base-washing when compared to GO-HOm, although not as high as it would be expected. As a consequence, large GO sheets obtained from the intercalation and oxidation of a graphitic material are less oxidized than it was believed, with a clear and dominant sp^2 aromatic structure, where the more abundant groups corresponds to ether-epoxy bands and carbonyl and carboxylic groups in a lower extent. Furthermore, OD-humic also exhibits a clear and dominant aromatic structure but with higher oxygen contributions, where now carbonyl, carboxylic and hydroxyl groups are more numerous than the 287.5 eV band. It is also important to note that the C/O ratio is slightly lower for OD-humic. This result and the mass spectrometry quantification suggest that the C/O value is not only due to the oxygen groups present in OD-humic, but also to the water retained by OD, as shown in TG.

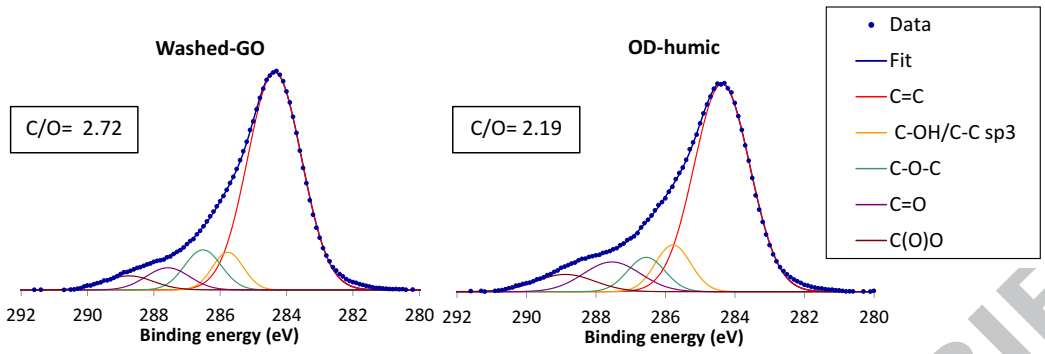

Figure 9. XPS C1s spectra of washed-GO and OD-humic

3.3.Model of graphene oxide

The analysis and characterization performed in this work allow us to propose a structural formation model for G-O. Results have shown clear differences among GO obtained by different oxidation methods and, therefore, different models are needed. Two main models are proposed for GO obtained by the Hummers-Offeman method ($KMnO_4/H_2SO_4/ NaNO_3$) and by the Brodie approach ($KClO_3/HNO_3$) (see Figure 10).

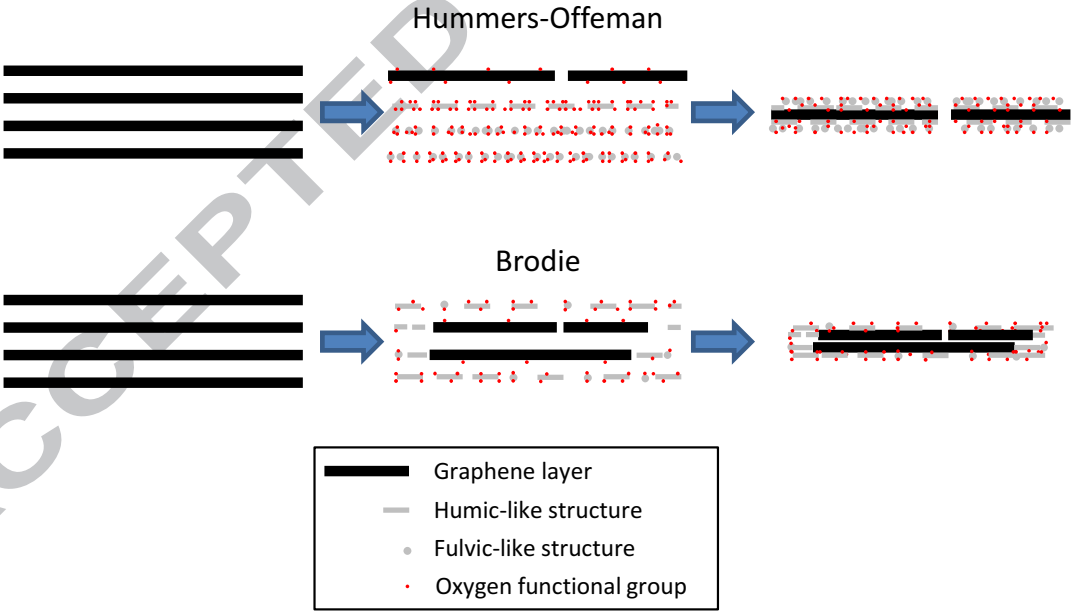

Figure 10. Proposed models for G-O

The initial graphitic structure is represented by 4 layers shown at the top left of Figure 10. The experiments considering $KMnO_4$ and H_2SO_4, result in the effective intercalation and simultaneous formation of around 20-30% of observable large sheets, oxidized

slightly at the basal plane and in a higher extent at the edges. At the same time, the cutting action also forms a set of low and very low fully oxidized planes, substances or molecules, with a high O/C ratios caused by the large edge to surface ratio. Soon after, $NaNO_3$ helps $KMnO_4$ to penetrate into the graphite layers. Following exfoliation, GO obtained by Hummers-Offeman method consists of a GO sheet with adhered humic and fulvic-like structures and high oxygen groups (see Figure 10).

In Brodie method, due to the superficial effect of HNO_3, the breakage is mainly produced only in outer layers and edges of graphite, and there is not a good intercalation of HNO_3 within the inner layers. Moreover, $KClO_3$ has an oxidation effect more limited than $KMnO_4$, and does not cut the basal plane like the Hummers method. Therefore, there is a reduced formation of humic and fulvic-like structures and, after exfoliation, most of the GO sheets are not individualized. The structure of GO obtained by the Brodie method consists of a few GO sheets (not exfoliated) with a low amount of humic and fulvic-like molecules adhered to the top and the bottom, and lower oxygen content.

4. Conclusions

We studied the structure of GO synthesized using different routes. In particular, we quantified and characterized the washed GO fractions, containing the clean GO sheets and oxidative debris, and further analyzed the humic-like fractions. When oxidizing natural graphite, the nature and amount of the resulting washed-GO sheets and humic-like fractions are different depending on the synthesis method. Our main conclusions are shown below:

- The Hummers and Offeman method yields the most satisfactory graphite exfoliation among the different reaction methods: over 50% of single layers in the as-produced GO, and subsequent full exfoliation after thermal treatment. The content of clean GO sheets is as low as 20%, whereas the humic-like material reaches *ca.* 30% of the total as-produced GO. There is still another 50% formed by fulvic-like compounds and trapped intercalated sulfuric acid and water.
- The intercalation and the reaction of $KMnO_4$, with the aid of sulfuric acid and sodium nitrate, produces mainly “scissor-like” cutting of the basal planes, thus resulting in a complex mixture of *sheets* of widespread sizes, with edges being

fully oxidized with phenol, lactone, ketone and carboxylic groups. The fulvic-like fractions correspond to the smallest size *sheets* (molecule size), humic-like species to medium size layers (roughly 5-50 nm), and finally clean GO sheets. Agglomerated humics shows an amorphous gel texture, with intermediate oxygen content trapped in between clean sheets and as-produced GO.

- When $NaNO_3$ is not present, the $KMnO_4$ is less effective, thus resulting in a washed GO fraction with low presence of humics. In parallel, it was detected that there were still present non-intercalated layers.
- The Brodie method with $KClO_3$ in nitric acid shows a different exfoliation mechanism and resulting GO product when compared to the Hummers-Offeman method. It results in a highly oxidation process, but it only takes place superficially, with poor reactive intercalation in between the layers: the water content is low and does not play a role upon thermal decomposition, and the sum of the humic and fulvic-like fractions is very little (*ca.* 20%) with respect to the washed GO (*ca.* 80%). In addition, the Brodie-based GO shows oxygen groups in the basal plane, according to the higher shifts in the Raman G-band.
- It is possible to propose a more detailed model for the production of GO. In short, in order to be able to produce monolayers of GO in an effective way, the intercalation of oxidant and acid takes place if there is also an additional simultaneous "scissor-cutting" of the basal plane. In other words, when synthetizing GO through the Hummers and Offeman method, graphite is either converted into GO, and unavoidable consumed into oxidative debris. In addition, the Brodie method does not efficiently produce monolayer GO and does not converts graphite into oxidative debris.

Acknowledgements.

The authors thank the Government of Spain, Ministry for Economy and Competiveness, for financial support of project CTQ2013-44213-R, and Generalitat Valenciana for projects PROMETEOII/2014/007 and ISIC/2012/008. IRP thanks the Government of Spain, Ministry of Science and Education, for PhD Scholarship in the FPU program.

References.

[1] Li X, Cai W, An J, Kim S, Nah J, Yang D, et al. Large-area synthesis of high-quality and uniform graphene films on copper foils. Science. 2009;324(5932):1312-4.
[2] Hwang J, Kim M, Campbell D, Alsalman HA, Kwak JY, Shivaraman S, et al. van der Waals Epitaxial Growth of Graphene on Sapphire by Chemical Vapor Deposition without a Metal Catalyst. ACS Nano. 2012;7(1):385-95.
[3] Yang X, Dou X, Rouhanipour A, Zhi L, Räder HJ, Müllen K. Two-Dimensional Graphene Nanoribbons. J Am Chem Soc. 2008;130(13):4216-7.
[4] Novoselov KS, Geim AK, Morozov SV, Jiang D, Zhang Y, Dubonos SV, et al. Electric field in atomically thin carbon films. Science. 2004;306(5696):666-9.
[5] Hernandez Y, Nicolosi V, Lotya M, Blighe FM, Sun Z, De S, et al. High-yield production of graphene by liquid-phase exfoliation of graphite. Nat Nano. 2008;3(9):563-8.
[6] Paton KR, Varrla E, Backes C, Smith RJ, Khan U, O'Neill A, et al. Scalable production of large quantities of defect-free few-layer graphene by shear exfoliation in liquids. Nat Mater. 2014;advance online publication.
[7] Hummers Jr WS, Offeman RE. Preparation of graphitic oxide. J Am Chem Soc. 1958;80(6):1339.
[8] Kosynkin DV, Higginbotham AL, Sinitskii A, Lomeda JR, Dimiev A, Price BK, et al. Longitudinal unzipping of carbon nanotubes to form graphene nanoribbons. Nature. 2009;458(7240):872-6.
[9] Varela-Rizo H, Rodriguez-Pastor I, Merino C, Martin-Gullon I. Highly crystalline graphene oxide nano-platelets produced from helical-ribbon carbon nanofibers. Carbon. 2010;48(12):3640-3.
[10] Lv R, Cruz-Silva E, Terrones M. Building Complex Hybrid Carbon Architectures by Covalent Interconnections: Graphene–Nanotube Hybrids and More. ACS Nano. 2014;8(5):4061-9.
[11] Chen D, Feng H, Li J. Graphene oxide: Preparation, functionalization, and electrochemical applications. Chemical Reviews. 2012;112(11):6027-53.
[12] Pei S, Cheng H-M. The reduction of graphene oxide. Carbon. 2012; 50(9):3210-3228.
[13] Zhu Y, Murali S, Cai W, Li X, Suk JW, Potts JR, et al. Graphene and Graphene Oxide: Synthesis, Properties, and Applications. Advanced Materials. 2010;22(35):3906-24.
[14] Bonaccorso F, Lombardo A, Hasan T, Sun Z, Colombo L, Ferrari AC. Production and processing of graphene and 2d crystals. Materials Today. 2012;15(12):564-89.
[15] Stoller MD, Park S, Yanwu Z, An J, Ruoff RS. Graphene-Based ultracapacitors. Nano Letters. 2008;8(10):3498-502.
[16] Boland CS, Khan U, Backes C, O'Neill A, McCauley J, Duane S, et al. Sensitive, High-Strain, High-Rate Bodily Motion Sensors Based on Graphene–Rubber Composites. ACS Nano. 2014;8(9):8819-30.
[17] Hassoun J, Bonaccorso F, Agostini M, Angelucci M, Betti MG, Cingolani R, et al. An Advanced Lithium-Ion Battery Based on a Graphene Anode and a Lithium Iron Phosphate Cathode. Nano Letters. 2014;14(8):4901-6.
[18] Dreyer DR, Todd AD, Bielawski CW. Harnessing the chemistry of graphene oxide. Chem Soc Rev. 2014;43(15):5288-301.
[19] Hofmann U, Holst R. Über die Säurenatur und die Methylierung von Graphitoxyd. Berichte der deutschen chemischen Gesellschaft (A and B Series). 1939;72(4):754-71.
[20] Ruess G. Monatshefte für Chemie. 1946;76:381-417.
[21] Scholz W, Boehm HP. Untersuchungen am Graphitoxid. VI. Betrachtungen zur Struktur des Graphitoxids. Zeitschrift für anorganische und allgemeine Chemie. 1969;369(3-6):327-40.
[22] Nakajima T, Mabuchi A, Hagiwara R. A new structure model of graphite oxide. Carbon. 1988;26(3):357-61.

[23] Lerf A, He H, Forster M, Klinowski J. Structure of graphite oxide revisited. Journal of Physical Chemistry B. 1998;102(23):4477-82.
[24] He H, Klinowski J, Forster M, Lerf A. A new structural model for graphite oxide. Chemical Physics Letters. 1998;287(1–2):53-6.
[25] Dreyer DR, Park S, Bielawski CW, Ruoff RS. The chemistry of graphene oxide. Chem Soc Rev. 2010;39(1):228-40.
[26] Seredych M, Tamashausky AV, Bandosz TJ. Graphite Oxides Obtained from Porous Graphite: The Role of Surface Chemistry and Texture in Ammonia Retention at Ambient Conditions. Advanced Functional Materials. 2010;20(10):1670-9.
[27] Brodie BC. XXIII. - Researches on the atomic weight of graphite. Quarterly Journal of the Chemical Society of London. 1860;12(1):261-8.
[28] Chua CK, Sofer Z, Pumera M. Graphite oxides: Effects of permanganate and chlorate oxidants on the oxygen composition. Chemistry - A European Journal. 2012;18(42):13453-9.
[29] Staudenmaier L. Ber Dtsch Chem Ges. 1898;31:1481-7.
[30] Marcano DC, Kosynkin DV, Berlin JM, Sinitskii A, Sun Z, Slesarev A, et al. Improved Synthesis of Graphene Oxide. ACS Nano. 2010;4(8):4806-14.
[31] Rourke JP, Pandey PA, Moore JJ, Bates M, Kinloch IA, Young RJ, et al. The Real Graphene Oxide Revealed: Stripping the Oxidative Debris from the Graphene-like Sheets. Angewandte Chemie International Edition. 2011;50(14):3173-7.
[32] Fogden S, Verdejo R, Cottam B, Shaffer M. Purification of single walled carbon nanotubes: The problem with oxidation debris. Chem Phys Lett. 2008;460(1-3):162-7.
[33] Verdejo R, Lamoriniere S, Cottam B, Bismarck A, Shaffer M. Removal of oxidation debris from multi-walled carbon nanotubes. Chemical Communications. 2007(5):513-5.
[34] Wu Z, Pittman Jr CU, Gardner SD. Nitric acid oxidation of carbon fibers and the effects of subsequent treatment in refluxing aqueous NaOH. Carbon. 1995;33(5):597-605.
[35] Thomas HR, Day SP, Woodruff WE, Vallés C, Young RJ, Kinloch IA, et al. Deoxygenation of Graphene Oxide: Reduction or Cleaning? Chemistry of Materials. 2013;25(18):3580-8.
[36] Faria AF, Martinez DST, Moraes ACM, Maia Da Costa MEH, Barros EB, Souza Filho AG, et al. Unveiling the role of oxidation debris on the surface chemistry of graphene through the anchoring of ag nanoparticles. Chem Mater. 2012;24(21):4080-7.
[37] Thomas HR, Vallés C, Young RJ, Kinloch IA, Wilson NR, Rourke JP. Identifying the fluorescence of graphene oxide. Journal of Materials Chemistry C. 2013;1(2):338-42.
[38] Coluci VR, Martinez DST, Honório JG, De Faria AF, Morales DA, Skaf MS, et al. Noncovalent interaction with graphene oxide: The crucial role of oxidative debris. Journal of Physical Chemistry C. 2014;118(4):2187-93.
[39] Wang Z, Shirley MD, Meikle ST, Whitby RLD, Mikhalovsky SV. The surface acidity of acid oxidised multi-walled carbon nanotubes and the influence of in-situ generated fulvic acids on their stability in aqueous dispersions. Carbon. 2009;47(1):73-9.
[40] Dimiev AM, Alemany LB, Tour JM. Graphene oxide. Origin of acidity, its instability in water, and a new dynamic structural model. ACS Nano. 2013;7(1):576-88.
[41] Steurer P, Wissert R, Thomann R, Mülhaupt R. Functionalized graphenes and thermoplastic nanocomposites based upon expanded graphite oxide. Macromolecular Rapid Communications. 2009;30(4-5):316-27.
[42] Dresselhaus M, Dresselhaus SG. Intercalation Compounds of Graphite Advances in Physics. 1981;30:290.
[43] Kaniyoor A, Ramaprabhu S. A Raman spectroscopic investigation of graphite oxide derived graphene. AIP Advances. 2012;2(3):032183-13.
[44] Ganguly A, Sharma S, Papakonstantinou P, Hamilton J. Probing the Thermal Deoxygenation of Graphene Oxide Using High-Resolution In Situ X-ray-Based Spectroscopies. The Journal of Physical Chemistry C. 2011;115(34):17009-19.

[45] Gouadec G, Colomban P. Raman Spectroscopy of nanomaterials: How spectra relate to disorder, particle size and mechanical properties. Progress in Crystal Growth and Characterization of Materials. 2007;53(1):1-56.
[46] Stankovich S, Dikin DA, Piner RD, Kohlhaas KA, Kleinhammes A, Jia Y, et al. Synthesis of graphene-based nanosheets via chemical reduction of exfoliated graphite oxide. Carbon. 2007;45(7):1558-65.
[47] Eigler S, Dotzer C, Hof F, Bauer W, Hirsch A. Sulfur Species in Graphene Oxide. Chemistry – A European Journal. 2013;19(29):9490-6.
[48] Liu H, Zhang Y, Li R, Sun X, Abou-Rachid H. Thermal and chemical durability of nitrogen-doped carbon nanotubes. Journal of Nanoparticle Research. 2012;14(8).
[49] Compton OC, Jain B, Dikin DA, Abouimrane A, Amine K, Nguyen ST. Chemically active reduced graphene oxide with tunable C/O ratios. ACS Nano. 2011;5(6):4380-91.
[50] Larciprete R, Gardonio S, Petaccia L, Lizzit S. Atomic oxygen functionalization of double walled C nanotubes. Carbon. 2009;47(11):2579-89.
[51] Poh HL, Sanek F, Ambrosi A, Zhao G, Sofer Z, Pumera M. Graphenes prepared by Staudenmaier, Hofmann and Hummers methods with consequent thermal exfoliation exhibit very different electrochemical properties. Nanoscale. 2012;4(11):3515-22.